Geochimica et Cosmochimica Acta, Vol. 69, No. 7, pp. 1651–1663, 2005

0016-7037/05 $30.00 + .00

doi:10.1016/j.gca.2004.07.038

Direct observation of heavy metal-mineral association from the Clark Fork River Superfund Complex: Implications for metal transport and bioavailability

Michael F. Hochella Jr.,[1,*], Johnnie N. Moore[2], Christine V. Putnis[3], Andrew Putnis[3], Takeshi Kasama[3†], Dennis D. Eberl[4]

[1]Nanogeoscience and Technology Lab, Department of Geosciences, Virginia Tech, Blacksburg, Virginia 24061 USA
[2]Department of Geology, University of Montana, Missoula, Montana 59812 USA
[3]Institüt für Mineralogie and Interdisciplinary Centre for Electron Microscopy and Microanalysis, Universität Münster, Corrensstr. 24, D-48149, Münster, Germany
[4]Water Resources Division, United States Geological Survey, 3215 Marine Street, Denver, Colorado 80303 USA

(*Received December* 29, 2003; *accepted in revised form July* 20, 2004)

Abstract—Two sets of samples from riverbeds and adjacent floodplains, separated by 80 river kilometers, were collected from the Clark Fork River Superfund Complex, Montana, (the largest Superfund site in the United States), and studied primarily with transmission electron microscopy (TEM) with several supporting techniques to determine heavy metal-mineral association. Seven of the eight samples studied were strongly influenced by material that once resided in mining and smelting dumps and impoundments; this material was transported downstream sometime during the last century and a half from the Butte/Anaconda areas. The eighth sample was from a deeper floodplain level and dates to premining days. The TEM observations afford a direct look, down to the nanometer level, at secondary mineral formation as a result of the breakdown of sulfides and silicates in the acid environment of this massive mine-drainage system. In the shallow, oxic floodplain sediments, heavy metals of concern in this system (As, Cu, Pb, and Zn) are taken up by the formation of sulfates (particularly Pb in jarosite), as well as hydrous metal oxides (As, Cu, Pb, and Zn in and on ferrihydrite, and a possibly new vernadite-like mineral). The oxides are long-lived in these systems, as they were also found in the anoxic riverbeds. Metals are also taken up by the formation of sulfides in sulfate-reducing environments as observed in the formation of nanoclusters of chalcopyrite and sphalerite. In all samples, clays make up between 5 and 20% of the sediment and carry significant amounts of Cu and Zn. The hydrous oxides, secondary sulfides, and clays provide several routes for metal transport downstream over long distances. Besides the potential bioavailability of heavy metals exchanged on and off the hydrous metal oxides and clays, nanometer-sized sulfides may also be highly reactive in the presence of biologic systems.

1. INTRODUCTION

Mining operations involving sulfide minerals generally result in the excavation of large quantities of rock from the anoxic subsurface and its transport to the surface oxic environment. This transformation results in the generation of acids and leaching of metals that are then transported into surface and groundwater systems. In the process, metal-rich particulate material is also supplied to streams and rivers, with latent deleterious reactions sometimes occurring decades to centuries later.

The amount of hazardous wastes released from base-metal mining and smelting operations (e.g., 10^{10} kg in the United States in 1985 alone; U.S. Environmental Protection Agency, 1985) and transported into rivers can be enormous (e.g., Maron, 1989; Moore and Luoma, 1990; Jambor and Blowes, 1994; Swanson, 2002). Therefore, mining wastes deposited on river floodplains and in river channels are a major component of riverine contamination (Moore and Luoma, 1990; Miller, 1997; Hudson-Edwards et al., 2003) and represent an important source of metal toxicity to aquatic and riparian biota (Axtmann and Luoma, 1991; Luoma and Carter, 1991; Lejeune et al., 1996). Mining wastes affect drainage basins throughout the world and degrade surface water resources in over 20,000 km of streams in the United States alone (DaRosa and Lyon, 1997).

Especially in older mining operations, waste rock still containing sulfides, as well as smelter waste, was commonly dumped directly into or near river and stream channels. Floods and channel aggregation transport these wastes downstream and deposit them on floodplains (Miller, 1997; Hudson-Edwards et al., 2003). On the floodplains, sulfides are oxidized in place and are transformed via microbial and inorganic reactions to oxic phases (sulfates, oxides, hydroxides and oxyhydroxides; e.g., Bigham, 1994; Bigham and Nordstrom, 2000). When the floodplain is eroded by channel migration, these new compounds and residual sulfides can then be eroded into the river and transported farther downstream (Swanson, 2002, and references therein). Therefore, over time wastes move through a mosaic of complex redox and pH environments that have profound effects on the solid and solute phases. It is important to understand these changes and phases, because they ultimately control bioavailability, and hence, toxicity of the metals to aquatic organisms, insects, and potentially mammals, including humans.

In a previous study of mining wastes (Hochella et al., 1999), we set out to determine heavy metal-mineral associations down to the nanometer scale, relying primarily on transmission electron microscopy (TEM) and energy dispersive X-ray (EDX)

* Author to whom correspondence should be addressed (hochella@vt.edu).
† *Present address:* Department of Materials Science and Metallurgy, University of Cambridge, Pembroke St., Cambridge, CB2 3QZ, UK

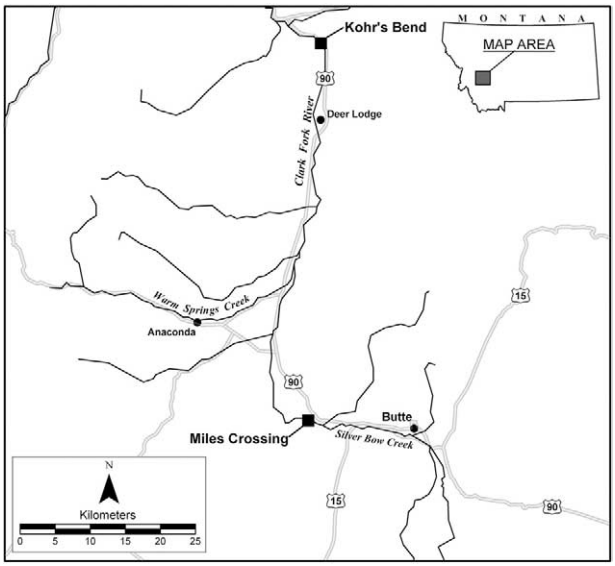

Fig. 1. Map of the headwaters of the Clark Fork River in Montana, USA (state outline in upper right with box showing the position of the expanded portion). The locations of Butte and Anaconda are shown, as well as the Miles Crossing and Kohr's Bend sampling locations. Smelter and mining waste dumps cover many tens of square kilometers in both the Butte and Anaconda areas.

analysis. In the present study, these methods are applied to the problem of how metals are bound in different environments as they move through an actual drainage system. We examined a set of eight samples from contaminated floodplains and bed sediments along/in Silver Bow Creek and the Clark Fork River, Montana, (Fig. 1). These waterways are part of the country's largest Superfund site, the Clark Fork River Superfund Complex generated by very large-scale base metal mining operations for nearly one and a half centuries (see Moore and Luoma, 1990, for a detailed description of this site). The objectives were to determine how metals are bound in weathered, contaminated floodplain soils in different horizons, examine how that compares to the premining soil horizons beneath the deposited tailings, and to determine how these same metals are bound once eroded and deposited in anoxic stream channel environments. The ultimate goal of this type of detailed, direct nanoscale observation of metal contaminants is to better describe the system and processes within it so that we can understand the conditions that will fix and/or mobilize contaminants from floodplain and stream sediments.

To accomplish these objectives and reach this goal, we analyzed more than 80 ultramicrotome thin sections in the TEM from the eight sampling locations. This helped assure that our TEM observations were representative of each sample as a whole, thus overcoming a common problem with TEM-based studies. This assertion is supported by the fact that the major mineralogy determined by the sum of all TEM observations qualitatively agreed with the major mineralogy as determined by powder X-ray diffraction (XRD) and scanning electron microscopy (SEM)/energy dispersive X-ray (EDX) analysis. Beyond this, the TEM provided additional and often unique observations on the minor and trace minerals that are so important in this system because of their association with heavy metals. It is these observations that form the basis of this contribution.

2. SAMPLES AND METHODS

2.1. Sampling Locations, Sample Naming, Handling, and Initial Observations

The first sample set was collected on Silver Bow Creek at a location called Miles Crossing, 3 km west from the Ramsey Exit off Interstate 90 and ~15 km west of Butte, Montana (Fig. 1). Digging into the side of the 1 m high vertical riverbank (cutbank) with a trowel revealed two distinct layers of floodplain sediments. The two layers were slightly different shades of brown with fine reddish streaks going through them. The material was loosely compacted and very slightly damp. Approximately 250 g samples were collected from each layer at depths of 15 and 30 cm below the floodplain surface (designated MC-1 and MC-2, respectively). Also at this location, two riverbed samples a few meters apart were collected (designated MC-3 and MC-4). These samples were near the stream edge with a water depth of 10 to 20 cm. The samples consisted of a fine black mud that was found under a thin layer of much coarser, light-brown sediment less than 1 cm thick that formed the uppermost portion of the riverbed in that location.

The second set of samples was collected ~80 river km downstream on the Clark Fork River. This location, known as Kohr's Bend, is just off Interstate 90 at the Beck Hill exit, ~64 km north, northwest of Butte (Fig. 1). Digging into the edge of the cutbank at this location revealed three distinct floodplain sediment layers (again distinguished by various shades of brown), so samples were collected at depths of 15, 30, and 50 cm corresponding to these levels (designated KB-1, KB-2, and KB-3, respectively). A single stream sediment sample was also collected near the edge of the river adjacent to the floodplain sampling position (designated KB-4). Again, the riverbed material collected was under ~20 cm of water, and the sample consisted of a fine black mud found under a medium brown mud, ~0.3 cm thick, forming the uppermost bed of the stream in this location.

All eight samples described above, weighing ~250 g each, were placed in plastic tubs and allowed to completely air-dry over the next several days before being capped for storage. Further, all samples were observed, as received, under a stereomicroscope. A portion of each sample was also imbedded in epoxy, and standard optical thin sections were made from these blocks.

2.2. Total Extractable Metal Analysis

A portion of each sample in this study was digested using an acid reflux (hydrochloric and nitric acids), and oxidation with hydrogen peroxide at 90°C (EPA Method 3050B). This method does an excellent job of accessing metals in sediments/soils that are considered "environmentally available." It is not considered a complete digest, but it dissolves all elements commonly of interest in mining-contaminated sediment. These elements include those tied to organic compounds and adsorbed to mineral surfaces, and those within metal sulfide, oxides, and hydroxides. The method will only partially dissolve silicate minerals, so elements in these minerals (Si, Al, Fe, Na, K, Mg, Ca, etc.) present in the effluent are not representative of the total elemental concentration in the sediment.

Once digested, the effluent for each sample was analyzed with an Inductively Coupled Argon Plasma Emission Spectrometer (ICP). EPA Method 200.7 was used for ICP analyses. This method includes a wide array of quality assurance efforts to insure the precision and accuracy of the data. The quality assurance measures include calibration blanks, blank and sample spikes, duplicates, and external standards.

2.3. Transmission Electron Microscopy

2.3.1. Sample preparation and mounting

TEM ultramicrotomed thin sections were prepared in a similar fashion to the method described in Hochella et al. (1999). Each sample was already highly friable, and therefore, satisfactory dispersion could be achieved with only light grinding. The samples were then dry sieved in a number of stages, finishing with <65 μm, and finally wet sieved

Table 1. Extractable metals and sulfur, in ppm.

	Location*	S	As	Cu	Pb	Zn
MC-1	Floodplain, 15 cm deep	262	BDL[#]	272	28	1007
MC-2	Floodplain, 30 cm deep	368	10	438	51	1428
MC-3	Riverbed	8340	400	6272	1015	4656
MC-4	Riverbed	7164	122	1024	447	1697
KB-1	Floodplain, 15 cm deep	1122	394	313	273	461
KB-2	Floodplain, 30 cm deep	861	725	5554	549	1423
KB-3	Floodplain, 50 cm deep	410	23	26	28	110
KB-4	Riverbed	773	24	249	53	409

MC = Miles Crossing on Silver Bow Creek; KB = Kohr's Bend on the Clark Fork River, 80 km downstream from MC.
* See text for details.
[#] Below detection limit.

in ethanol to <25 μm. A final light grinding was performed in an attempt to reduce the largest grains (mostly brittle quartz and feldspar) to a smaller size and to continue to disperse the sample as much as possible, both of which are important in improving the quality of the ultramicrotome cutting. The samples were then impregnated with epoxy, thinned by polishing to a thickness of 10 to 20 μm, and finally cemented into an epoxy block for ultramicrotome cutting with a diamond knife as described in Hochella et al. (1999). Final cut sections for this study were between 20 and 50 nm in thickness. The resulting films, floating on water in the trough of the diamond knife holder, were quickly recovered on 300 mesh nickel TEM grids. Finally, all sections/grids were lightly coated with carbon.

2.3.2. *Microscopy and chemical analysis*

A JEM-3010 (JEOL) TEM was used in this study at a beam energy of 300 kV with beam currents between 115 and 119 μA using a LaB_6 filament. The nickel grids were loaded onto a double-tilting analytical specimen holder (beryllium components) for observation. EDX analysis was performed with an Oxford Link ISIS system equipped with an atmosphere thin window for light element detection. Semiquantitative determination of key metal concentration ratios was performed using the Cliff-Lorimer ratio technique and k_{AB}-factors published in Williams and Carter (1996), and references therein.

Under the conditions noted above, beam damage was not observed for any of the phases studied except, on occasion, jarosite, illite/sericite, and smectite. In these cases, care was taken to limit beam exposure, and to collect image, diffraction, and EDX information quickly. Sample degradation was monitored by diffraction pattern quality and EDX-measured compositional changes with time. All data/images in this article are free of degradation artifacts.

2.4. Scanning Electron Microscopy

All eight samples in this study were studied extensively by SEM using primarily a JEOL JSM-6300F field emission microscope with an Oxford Instruments OX-2000 INCA system EDX analyzer. For a limited number of sessions, a JEOL JSM-840A microscope with a similar EDX analyzer was also used. Sample preparation consisted of gently breaking apart sample clots (the samples were not ground), and the resulting grains were dusted over Leit-C tabs on the SEM sample stubs. Before insertion into the SEM, each sample was lightly carbon-coated.

The few grains containing heavy metals (besides Fe-containing silicates) were located with backscattered electron (BSE) images that were collected at very low magnification over the dispersed-grain SEM mounts as described above. Typically, within the several square millimeter area that could be viewed at once, an area, or a few areas, of high backscattered electron intensity were apparent. Taking a number of BSE images while zooming in on the area helped locate nonsilicate grains that had a relatively high probability of containing heavy metals. In many cases, high resolution SEM imaging and EDX analysis resulted in identification of the grain or grains of interest.

2.5. Quantitative Powder X-ray Diffraction

Samples were prepared for XRD analysis according to the methods described by Srodon et al. (2001). Briefly, 3 g of sample were mixed with 0.333 g of an internal standard (zincite) and with 4 mL of methanol. The mixture was ground in a McCrone mill for 5 min, and then dried at 85°C. The powder then was sieved and side-loaded into an Al holder for X-ray analysis. Samples were X-rayed using a Siemens D500 diffraction system, with a Cu tube operated at 40 kV and 30 mA, and with a graphite monochromator. Samples were scanned from 5 to 65° two theta, with 0.02° two theta steps, and with a counting time of 5 s per step.

The XRD data were analyzed quantitatively for minerals present using the RockJock computer program (Eberl, 2003). RockJock offers a relatively simple and mostly automatic method for determining quantitatively the mineralogical composition of samples, including clay minerals, to within a few weight percent from powder XRD data. The calculations are based on three previously published methods: (1) the matrix flushing technique of Chung (1974), in which integrated intensities of the unknown minerals are compared to that of an internal standard (in the case of RockJock, ZnO), thereby obviating the need for measuring the mass absorption coefficient for a sample; (2) the whole-pattern fitting routine of Smith et al. (1987) for measuring integrated intensities by fitting the sum of pure mineral patterns to that of the measured XRD pattern, except that in RockJock, key parts of the patterns that contain the 060 reflections for clay minerals also are fitted separately; and (3) the quantitative method of Srodon et al. (2001) for sample preparation and for the method of measuring clay mineral content from 060 reflections rather than from the more commonly used basal reflections.

Table 2. Results of the quantitative XRD analysis for samples MC-4, KB-2, and KB-4.

	MC-4	KB-2	KB-4
Quartz	33	26	32
K-feldspar	19	10	18
Plagioclase	31	18	29
Amphibole	2	1	1
Pyroxene	1	1	1
Calcite	0	0	1
Pyrite	2	0	0
Jarosite	0	1	0
Magnetite	4	0	0
Hematite	1	1	0
Kaolinite	3	4	1
Nontronite	1	2	4
Illite + Muscovite + Al-rich smectite	1	16	6
Biotite	2	5	4
Chlorite	4	10	3
TOTAL	104	95	100

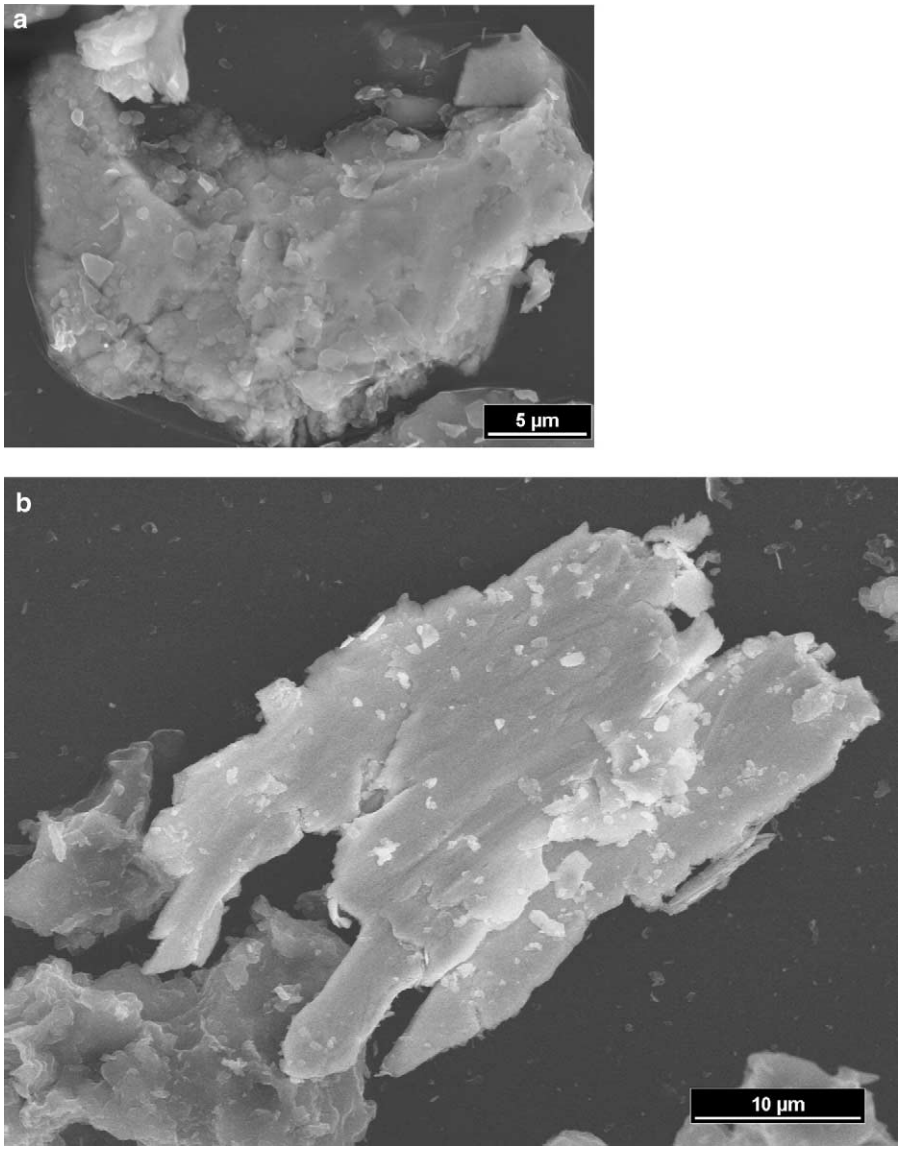

Fig. 2. (a) An SEM image of a grain of metallic Zn from the top layer of the Miles Crossing floodplain (MC-1); and (b) An SEM image of a metallic Cu grain from the second layer down in the Miles Crossing floodplain (MC-2). Both of these images show that these floodplain sediments are tailings from Anaconda/Butte smelting operations upstream.

3. RESULTS

3.1. Miles Crossing Samples

3.1.1. Optical, XRD, and extractable metals

The two samples from depths of 15 and 30 cm in the floodplain at Miles Crossing (MC-1 and MC-2, respectively), after drying, are both a light muddy brown color with rusty dull red-brown streaks throughout. MC-2 is slightly darker, overall, than MC-1. Grain size in both is generally less than 1 mm, and the material forms weakly bound clumps. In thin section, both samples exhibit angular grains of quartz and feldspar, and there are abundant sheet silicates as well. Opaque grains make up only ~1% in each, and the minerals in the fine groundmass are too minute for optical identification, except for the iron oxides with their characteristic color. Quantitative XRD analyses were not performed on these samples. The total extractable As, Cu, and Pb amounts (Table 1) are generally the lowest for all samples in this study except KB-3, the deepest of the floodplain samples collected at Kohr's Bend. The extractable S of both are the lowest of all samples studied.

The two samples from the riverbed at Miles Crossing (MC-3 and MC-4), after complete air drying, are both a medium gray-brown in color with a hint of green. Both are generally fine grained and loose, although MC-4 is more unsorted. Optical examination of the thin sections of MC-3 and MC-4 were similar to MC-1 and MC-2, although, as expected from the sample color, there are fewer iron oxides in MC-3 and MC-4. Quantitative XRD analysis of MC-4 is shown in Table 2. Quartz and the feldspars, as expected, account for over 80% of the sample. Sheet silicates make up another ~11%. The aver-

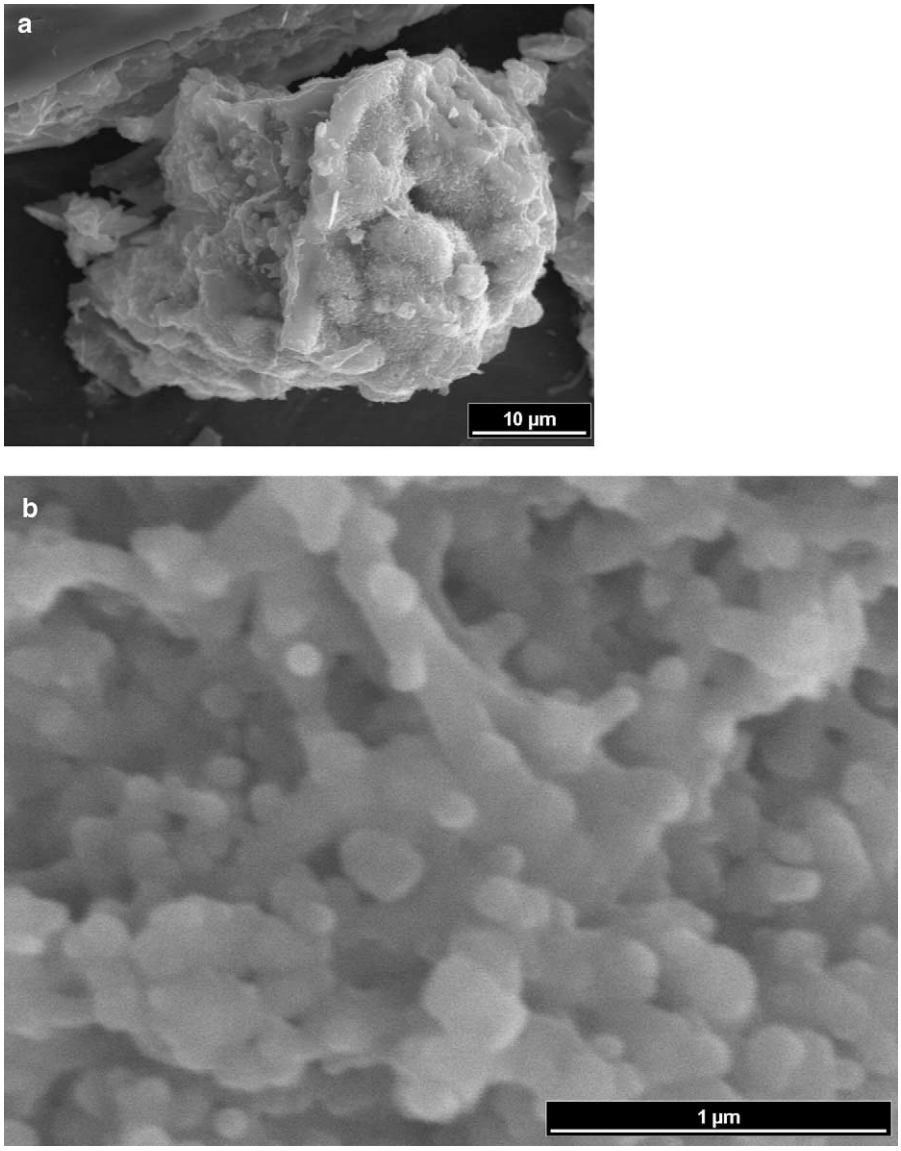

Fig. 3. (a) SEM image of a large silicate grain from the floodplain sediments at Miles Crossing (MC-1). The grain is covered, in part, by minute crystals of iron oxides, some of which are shown in (b).

age total extractable metal contents for both samples, for As, Cu, Pb, and Zn (Table 1), are the highest of all eight samples except for KB-2. The extractable S content of the two are the highest of all samples studied.

3.1.2. SEM/TEM results

The SEM observations of MC-1 and MC-2 agree well with the extractable metal content for each shown in Table 1. With moderate- to low-extractable heavy metal and relatively little sulfur, we did not expect to find many sulfide grains, and this was the case. However, these two floodplain beds are still clearly mine tailings and smelter wastes, and SEM evidence for this is shown in Figure 2a (a grain of metallic Zn; sample MC-1) and Figure 2b (a grain of metallic Cu; sample MC-2). Grains of iron oxides are also evident in the SEM. An example is shown in Figure 3, where a large silicate mineral grain (unidentified; Fig. 3a) is coated, at least in part, with minute iron oxide grains (Fig. 3b) that go down in size to the nanometer size regime (100 nm and less).

The TEM observations of MC-1 and MC-2 were the only portions of the TEM work in this entire study that did not seem to be fully representative of what we knew, or suspected to exist, from other parts of the study (SEM observations, optical examination, extraction data, etc.). Although a number of sections were studied, only quartz, feldspars, sheet silicates and clays, and occasionally some mafic silicate mineral grains were observed. And of the many clays that were studied in MC-1 and MC-2, none contained heavy metals besides Fe.

The SEM observations of MC-3 and MC-4, assisted greatly by BSE survey images as with all other samples, resulted in the location, imaging, and EDX analysis of a number of toxic heavy metal carrying sulfides, oxides, and metallic grains (the

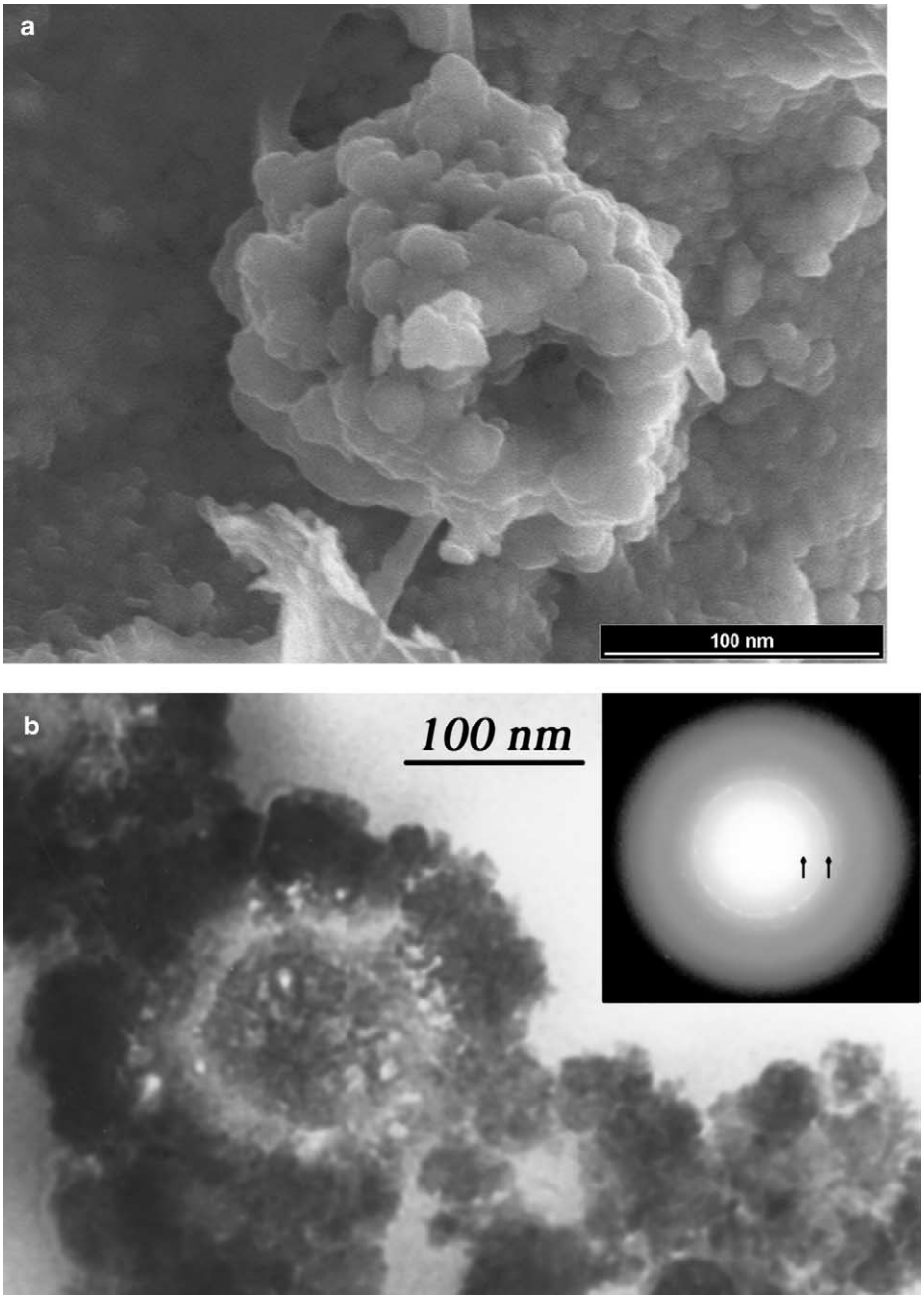

Fig. 4. (a) SEM image of a cluster of chalcopyrite crystals from the riverbed at the Miles Crossing site (MC-3); and (b) TEM image of presumably a similar occurrence of chalcopyrite crystal as (a), also from MC-3. Crystal sizes are as low as $<$10 nm, giving a weakly spotted ring diffraction pattern (the inner arrow points to the 3.03Å line, the outer to the 1.85Å line of chalcopyrite; the 1.59Å line is the very faint line just outside of this). Textural evidence suggests that these sulfides are secondary, growing in the anoxic environment of the riverbed.

latter including individual grains of a Cu, Zn alloy and an Fe, Ni, Cr alloy). These observations were not unexpected considering the high total extractable metal content, as well as the very high extractable S from these samples.

A particularly interesting SEM observation that relates directly to several TEM observations of the same samples, and has important implications for the distribution and transport of toxic metals in mining drainages, is shown in Figure 4a. This SEM image, taken at low voltage (5 kV) to enhance the surface feature observations and improve resolution, shows chalcopyrite grains with sizes down to less than 10 nm in a tight clump. The TEM view of chalcopyrite with the same morphology from the same sample is shown in Figure 4b. The importance of this common occurrence in these samples is explained in the Discussion section below.

Further TEM examination of many ultramicrotomed sections of MC-3 and MC-4 revealed a number of other phases in these samples that contain heavy metals. These phases include fer-

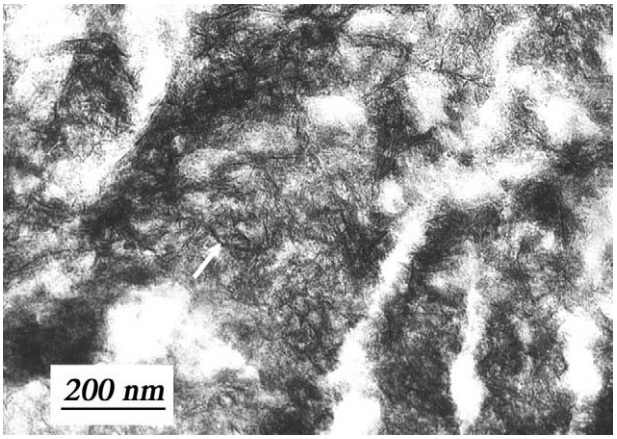

Fig. 5. The stippled areas (most of this TEM image) are nanocrystals of six-line ferrihydrite from the riverbed at Miles Crossing. The tiny dark "fibers" in the image (an arrow points to one) are a vernadite-like mineral (a Mn-oxide hydrate). See Discussion in this article and Hochella et al. (in press) for details on how these phases were identified.

rihydrite, various clays, and amorphous silica. Figure 5 shows a six-line ferrihydrite and a Mn hydrous oxide (Fe:Mn ratio ~9:1) from MC-4. Lesser amounts of Zn and As are also present with a (Fe+Mn):(Zn+As) ratio of ~10:1.

Although the clay content of MC-4 is not particularly high among these samples (on the order of 10%), many varieties were easily found throughout the TEM sections of this sample. Of particular interest are the clays that contain heavy metals. An example of a Zn-containing smectite (Si:Zn ~30:1) is shown is Figure 6.

Amorphous silica was also observed in several areas of two ultramicrotomed sections of sample MC-4 (Fig. 7a and b). This silica either shows no diffraction intensity whatsoever, or a single very faint and diffuse ring at a *d*-value of ~4Å. Besides Si and O, which dominate the EDX spectra, there is typically a considerable amount of Al and Fe present (Si:Al ~5:1; Si:Fe ~4:1), as well as minor amounts of Zn, K, Cl, K, Ca, Ti, and S. In Figure 7b, we also see nanocrystalline sphalerite within the amorphous silica.

3.2. Kohr's Bend Samples

3.2.1. Optical, XRD, and total extractable metal

Sample KB-1, from 15 cm deep in the floodplain at Kohr's Bend, after complete air-drying, is loose and a very light reddish brown. Sample KB-2, from 30 cm deep in the next layer down on the floodplain, is a medium brown color, fine, and consists of small loosely compacted clumps of grains as well as loose material. Sample KB-3, from 50 cm down in the lowest level studied, is a darker grey-brown, and also consists of small clumps as well as loose grains. In thin section, all three samples consist of a majority of quartz and feldspar as expected, but when going from KB-1 to KB-3, the amount of iron oxides and clays increase slightly and the groundmass becomes finer. Quantitative XRD was performed on sample KB-2, and it is made up of an estimated 54% combined quartz and feldspar, as well as 37% sheet silicates along with minor amounts of several other minerals (Table 2). The extractable As, Cu, Pb, and Zn (Table 1) are especially high for KB-2, but KB-3 is the lowest of all eight samples studied. Extractable S is moderate for KB-1 and KB-2, and low for KB-3.

The sample from the riverbed at Kohr's Bend (KB-4), after complete drying in air, is relatively unsorted and granular, and like MC-3 and MC-4, a slightly greenish grey-brown color. In thin section, it looks similar to KB-2, having a medium dark groundmass, but has more quartz and feldspar. Quantitative XRD (Table 2) shows nearly 80% quartz and feldspar, with only half the sheet silicates as in KB-2. The average total extractable metal is among the lowest for As and Pb for these eight samples. Cu is moderate in concentration among these samples and similar to MC-1 and KB-1, and Zn is relatively low and similar to KB-1. Extractable S for KB-4 is moderately high relative to all samples studied.

3.2.2. SEM/TEM results

Like the SEM study of the samples from Miles Crossing, the information gained from the Kohr's Bend samples via SEM is consistent with the extractable metal and S (Table 1). As before, BSE survey images were critical in initially locating grains that contained appreciable amounts of heavy metals. These grains were then identified by EDX analysis. KB-1 and KB-2, the top two floodplain levels studied at Kohr's Bend showing somewhat elevated to very high levels of extractable metals, contained grains of pure metal and alloys (Cu, Fe, Zn), sulfides (pyrite and chalcopyrite), sulfates (jarosites with and without Pb), and iron oxides. Conversely, as anticipated, we

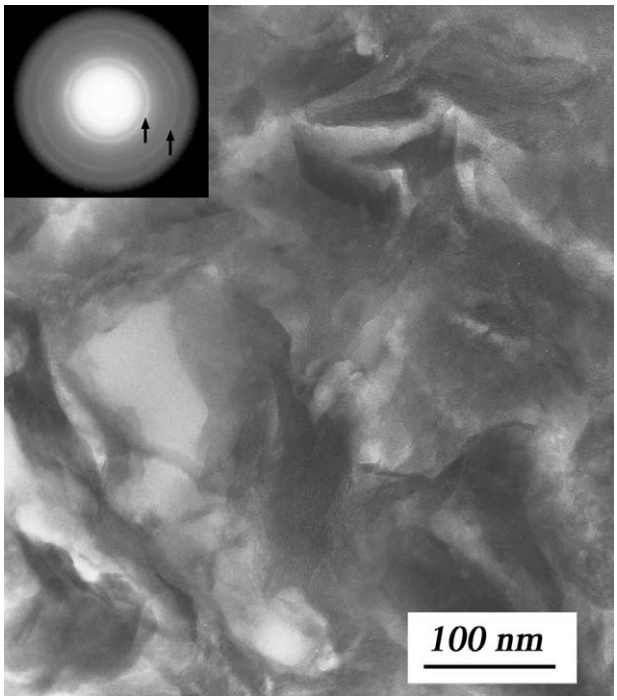

Fig. 6. Smectite from the riverbed at Miles Crossing. The whole field of view in this TEM image is made up of smectite as identified by EDX analysis and selected area diffraction patterns. The inner and outer arrows superimposed on the pattern shown indicate the 2.55 and 1.49Å lines of smectite, and the 4.55Å line is also easily observed at lower exposure times. This smectite contains a small amount of Zn.

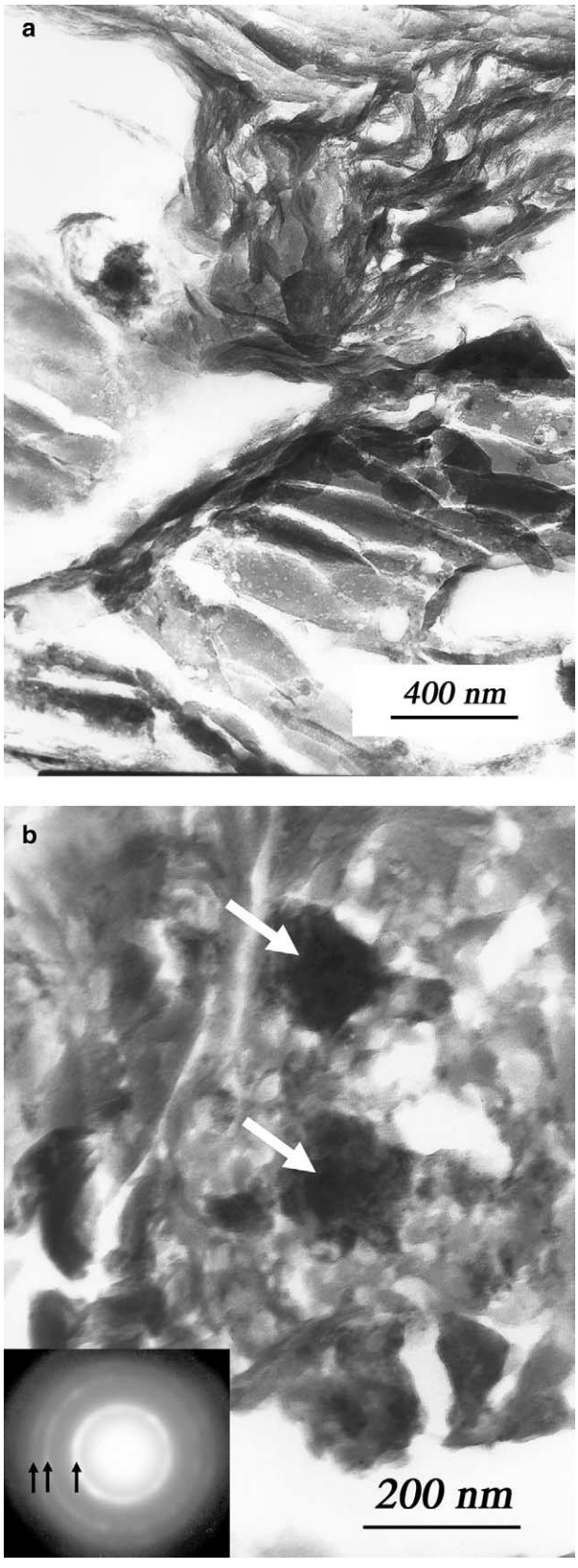

found no sulfides or sulfates in KB-3, the lowest floodplain level sampled at Kohr's Bend. However, Fe and Fe, Ti oxides were easy to find using BSE surveys.

The TEM studies of these three samples were generally consistent with the SEM observations. Sulfides, sulfates, and iron oxides were observed in the TEM for KB-1 and KB-2, but of these three heavy metal containing phases, only iron oxides were observed for KB-3. These iron oxides found in KB-3 do not include ferrihydrite, and of all those studied in that sample, none contain any metals besides Fe. Of particular interest are the jarosites (Fig. 8) and ferrihydrites (Fig. 9) studied from both KB-1 and KB-2. Figure 8a comes from sample KB-1, and shows jarosite crystals ($KFe_3(SO_4)_2(OH)_2$) with a small amount of Pb substituting for K except for one area, where Pb is clearly dominant over K (Fig. 8a, arrow). This crystal is close to the plumbojarosite stoichiometry ($Pb_{0.5}Fe_3(SO_4)_2(OH)_2$). Figure 8b is from KB-2, and shows a large field of jarosite crystals with approximately twice the amount of Pb substituting for K than the Pb-poor jarosites shown in Figure 8a. Figure 9 is from KB-1, and shows a field of both ferrihydrite (left, arrow) and jarosite (upper and lower right portions of the image). This ferrihydrite is the two-line variety, with some Mn present (Fe:Mn ratio ~10:1), and also small amounts of Pb, As, and a trace of Zn.

Clays are abundant in the ultramicrotomed sections of KB-1, KB-2, and KB-3 studied by TEM, agreeing with the quantitative XRD results for KB-2, and the optical examination of all three. In particular, sericite and smectite (and in several cases nontronite, an Fe^{3+}-rich smectite) were observed often. While nonclay sheet silicates in all of these samples are also present, EDX never showed them to contain heavy metals besides Fe. However, the clays found in all three of these samples commonly did. An example of nontronites from KB-2 containing small amounts of Cu (Fe:Cu ~12:1) is shown in Figure 10. Zn was also commonly found in clays in these samples, although it was not uncommon to find clays in all of these samples that did not have Cu, Zn, or any other heavy metal besides Fe.

The sample from the riverbed at Kohr's Bend showed moderate to low total extractable metal and S content, as mentioned above, but BSE surveying was still successful at finding the sulfides and iron oxides that were present. One SEM image from KB-4 is particularly illustrative of this. Figure 11 shows an alkali, alkaline-earth aluminosilicate grain (specific mineral unknown) with a number of minute grains covering portions of its surface. EDX analysis suggests that these grains are chalcopyrite and iron oxides. The TEM study of several ultramicrotomed sections of KB-4 showed similar results, although one

Fig. 7. TEM images of amorphous silica from the riverbed at Miles Crossing (MC-4). The whole field in (a) is amorphous silica with moderate to lesser amounts of Al and Fe, depending on exactly where the EDX spectra is collected, and lesser (minor) amounts of at least several of the following: Zn, K, Cl, K, Ca, Ti, and S. The same is true in (b), except the two darker masses indicated by white arrows have very different chemistry and show a smooth ring to diffusely spotted ring diffraction pattern, inserted in the bottom left corner. EDX shows these areas to be rich in Zn and S, but also with considerable, but lesser amounts of Si and O, and minor Fe, Pb, and As. The diffraction pattern matches that of sphalerite (the inner, middle, and outer arrows indicate the 3.12, 1.91, and 1.63Å lines of sphalerite).

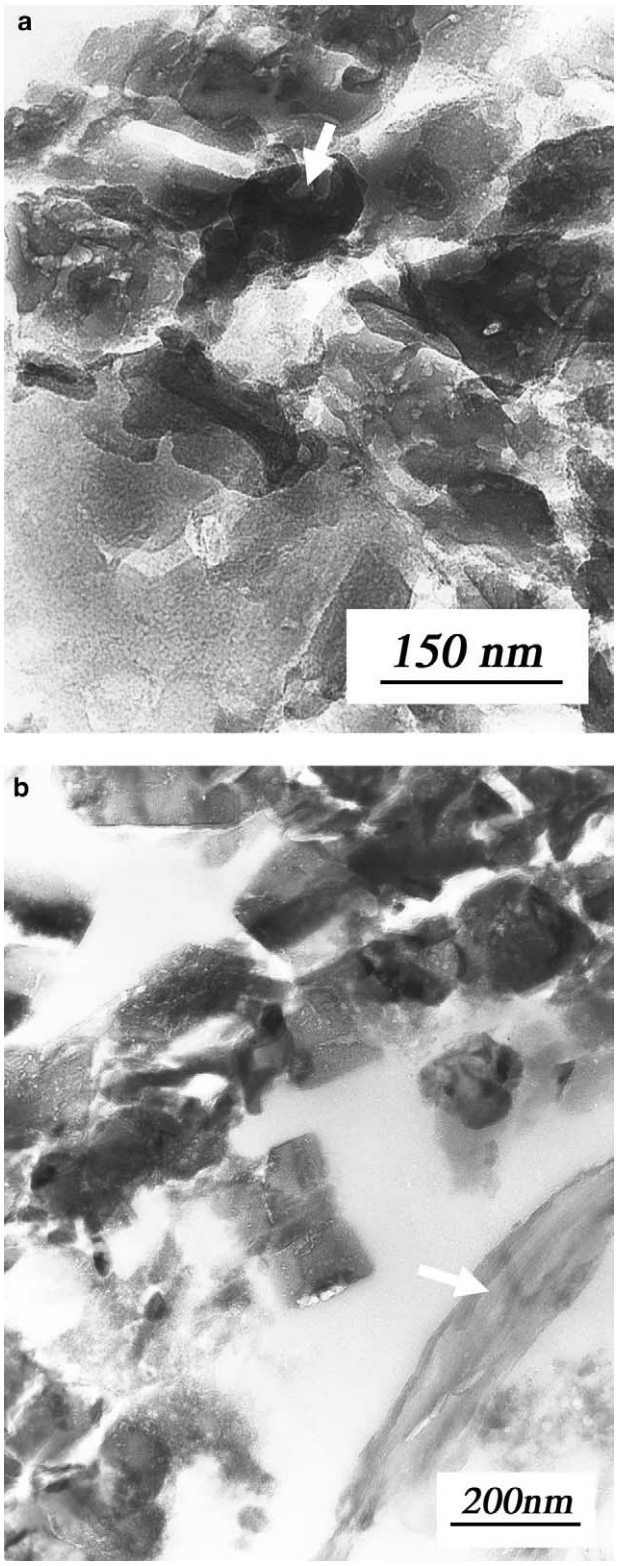

Fig. 8. (a) TEM image of a field of jarosite crystals from KB-1. The entire image has only jarosite crystals (identified by selected area diffraction patterns and EDX analysis) except for the medium grey stippled area filling up the lower left portion of the field of view. This area is amorphous aluminosilicate with small amounts of Fe, and no other elements. All jarosites in this image have a small amount of Pb substituting for K, except for the dark, 150 nm crystal marked by the arrow, which is close to the stoichiometry of plumbojarosite; and (b) TEM image of Pb-bearing jarosites (about twice the amount of Pb substitution as the low-Pb jarosite crystals in (a) from the floodplain at Kohr's Bend (sample KB-2). The only area in this image that is not jarosite is the lower right portion (arrow). This grain has no diffraction pattern, and is an Fe, Al silicate in composition.

of the oxides found is particularly interesting. This phase, described in detail in Hochella et al. (in press), is a poorly crystalline manganese oxide that may be similar to the mineral vernadite, a layered hydrous Mn oxide. Zn, and lesser amounts of As and Pb, are associated with this phase. One sulfide found by TEM was also interesting for similar reasons to the chalcopyrite in MC-3 and MC-4 described above, and interpreted below. In KB-4, this is a Zn-sulfide that forms exceptionally fine grains and thin films (Fig. 12). Because we could not obtain a diffraction pattern from this material, it is either amorphous, or there is too little material to give a visible diffraction pattern. Clays were also commonly seen in KB-4 with the TEM, as anticipated by the 20% clay content indicated by quantitative XRD (Table 2). Finally, although not shown in any of the figures, KB-4 contains amorphous silica with significant Al and Fe, and also minor amounts of Zn.

4. DISCUSSION

In this study, the TEM and other supporting techniques have painted a familiar story, then added critical details that provide new issues to consider in our understanding of these kinds of systems. Considering all samples examined in this study, one sees silicates, sulfides, and metal slag breaking down in the oxidizing and often low-pH zones of the floodplain sediments, releasing silica, alumina, metals and sulfate to solution, leading to the formation of (1) metal oxides, (2) sulfates, and (3) amorphous silica. In the anoxic streambeds, we have observed again metal oxides and amorphous silica, but also the formation of new sulfides. And in all samples, an abundance of clays are observed. All of these phases contain metals of biologic interest (in this case due to their toxicity). Each of these is discussed briefly below, based on the unique TEM results of this study.

4.1. Metal Oxides

The secondary metal oxides in this system, and that were observed in both the floodplain (where they form) and in the riverbed (where they persist), are poorly crystalline Fe,Mn hydrous oxides. These minerals include two- and six-line ferrihydrite (nominally $5Fe_2O_3 \cdot 9H_2O$) and a possibly new Mn hydrous oxide that may be similar to vernadite (see Hochella et al. (in press) for details on this phase). All have a great propensity for sorbing heavy metals of interest (in this system, every one studied has sorbed three or more of As, Cu, Pb, and Zn), and their persistence provides one avenue for heavy metal transport over long distances, as seen in this study. It is also interesting to note that crystalline Fe-oxides, including goethite, hematite, and wustite, were only rarely seen, and even if they were microcrystalline, contained no other metals besides Fe.

Other new factors to contemplate are the heavy metal uptake characteristics of the ferrihydrite vs. the vernadite-like mineral.

Fig. 9. TEM image of ferrihydrite and jarosite from the floodplain at Kohr's Bend (sample KB-2). The ferrihydrite, the wedge on the left side of the image denoted by the arrow, is the two-line variety with small amounts of Mn, Pb, and As present (see Hochella et al. (in press) for identification details). Jarosite crystals make up the right side of the image.

Recently, O'Reilly and Hochella (2003) looked at the Pb sorption efficiencies of several Fe- and Mn-oxides. Lead sorption ability of each reacting solid was normalized to its surface area. It was determined that ferrihydrite was no more reactive (per surface area) than any other Fe-oxide studied. However, two of the Mn-oxides tested, birnessite and cryptomelane, were significantly to dramatically more reactive per surface area. It is suggested in O'Reilly and Hochella (2003) that this is due to internal reactive sites in these structures (birnessite has a layer structure and cryptomelane has a 2×2 tunnel structure, and the structure of internal reactive sites has been studied in detail by, for example, Manceau et al., 2002). Vernadite was not tested in O'Reilly and Hochella (2003). However, its structure is described as a variation of the birnessite layer structure, except that it is disordered in the layer stacking direction (e.g., Post, 1999). If this is the case for the vernadite-like Mn-oxide found in the KB-2 and KB-4 samples, like birnessite, it will have a dramatically larger sorption capacity for Pb and other metals of interest relative to ferrihydrite. In fact, the EDX analyses of vernadite-like oxides from KB-2 showed twice or more of the amounts of As, Cu, Pb, and Zn as a pure ferrihydrite from the same sample (Hochella et al., in press).

4.2. Sulfates

The sulfate that dominates in these tailings-contaminated floodplain sediments is jarosite. This phase is so important environmentally because its structure readily takes up Pb (e.g., Alpers et al., 1994; Stoffregen et al., 2000). Jarosites with small to moderate amounts of Pb were common, and in one case, plumbojarosite was observed (Fig. 8). This variability in jarosite Pb chemistry has been seen before in other acid mine drainage sites (Hochella et al., 1999). Jarosites are only stable under low-pH conditions, from below pH 2 to 3 to less than pH 4 or 5 for plumbojarosite and in oxic zones (see Hochella et al., 1999, for a complete discussion). Consistent with this, in the present study jarosite was found in the floodplain sediments originating from mine tailings and smelter wastes, but not in the anoxic environment of the riverbeds. In the floodplain, when the pH rises in the interstitial solutions even locally, jarosites are unstable and will release Pb. Ferrihydrite is an excellent scavenger of Pb at pHs above ~5.5 (Benjamin and Leckie, 1981a; Benjamin and Leckie, 1981b). In the pH window between jarosite breakdown and ferrihydrite uptake, the Pb may remain aqueous and fully bioavailable.

4.3. Clays

This study shows that clays must be considered in metal transport and bioavailability studies of the Clark Fork system, and perhaps many other similar systems. Sericite (a very fine muscovite) and the smectites observed in this study (e.g., Figs. 6 and 10) are products of hydrothermal alterations of feldspars and are common in the mineralized veins from which Butte's copper production has come (Meyer et al., 1968; Page and Wenk, 1979). The minor amount of Cu and Zn in many of these

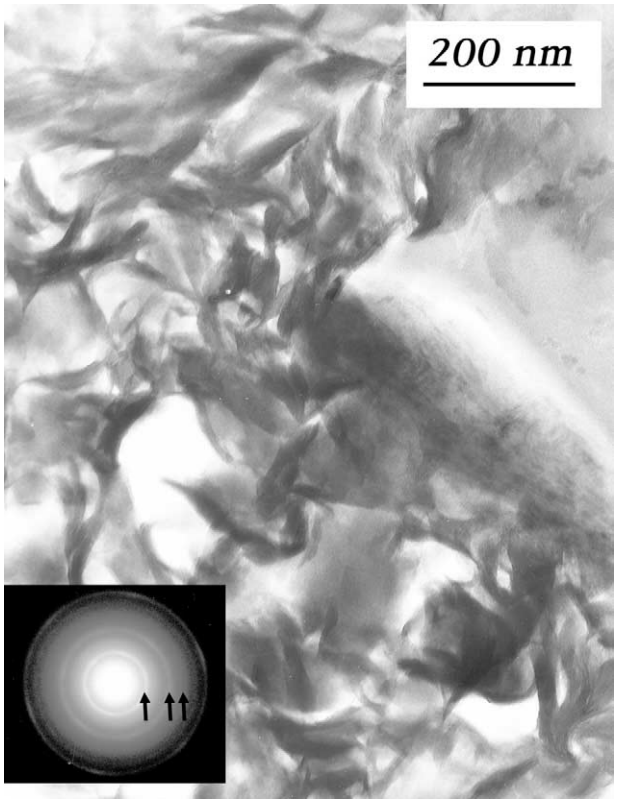

Fig. 10. TEM image of nontronite (an Fe-rich smectite) from the floodplain at Kohr's Bend (sample KB-2). The entire field of view is nontronite. The inner, middle, and outer arrows superimposed on the diffraction pattern show rings at the nontronite *d*-values of 4.56, 2.55, and 1.52Å, respectively. This nontronite contains a small amount of Cu.

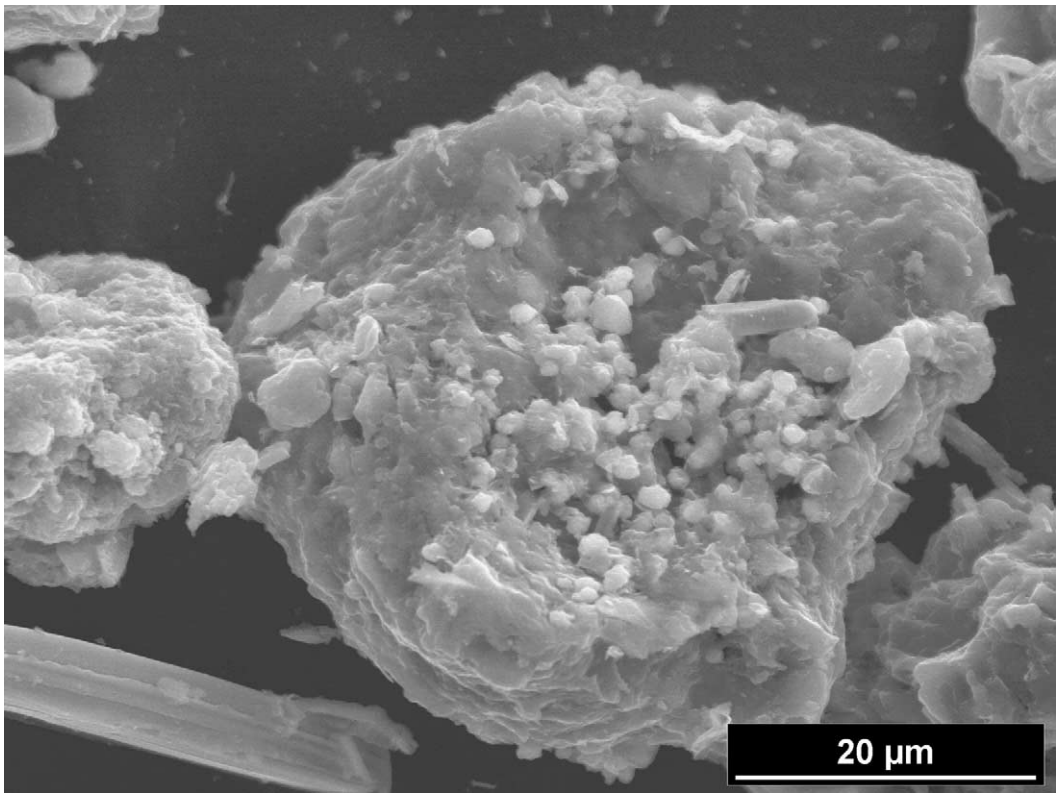

Fig. 11. SEM image of material from the riverbed at Kohr's Bend (sample KB-4). EDX indicates that the large grain at the center is an alkali-alkaline earth aluminosilicate (specific mineral is unknown), and the small grains covering part of its surface are chalcopyrite and iron oxides.

clays masks their importance as metal carriers: (1) the three samples analyzed by quantitative XRD have clay content between ~5 and 20% (Table 2). TEM observations show that clays make up major portions of the other five samples as well; and (2) Cu and Zn can reside in the octahedral layer with Fe, but it is also possible that some may reside in the interlayer of the smectites. More study is needed to see if this latter possibility is the case. If it is, some of the metals in these smectites could be exchangeable, and therefore, bioavailable.

4.4. Amorphous Silica

Amorphous silica was frequently observed in the Hochella et al. (1999) study, and it was again in this study. We found amorphous silica in half the samples studied, from both the floodplain sediments (originating from mine tailings) and the samples from the riverbeds. This material may have a biogenic origin, or it could be inorganically derived. In either case, it is an important breakdown product from silicates in these systems. In this study, the silica was observed to contain variable but substantial amounts of Al, Fe, and sometimes small quantities of Zn, although pure silica was also observed. All of this material may be hydrated as well. The presence of Al in much of this amorphous silica deserves special note. There has been considerable interest in Al in mine drainage systems (e.g., Jambor, 1994; Kimball et al., 1994; Hochella et al., 1999), considering its toxicity to aquatic life, even at very low concentrations, as well as its relative immobility. The amorphous silica holding Al in our samples is probably destined to crystallize as clays, but between the breakdown of primary aluminosilicate minerals and clay formation, this amorphous silica presumably limits the bioavailability of Al.

4.5. Secondary Sulfides

We also found direct evidence of secondary sulfides forming in the anoxic zones of the riverbed at the Miles Crossing site (MC-3 and MC-4) and the Kohr's Bend site (KB-4). In MC-3 and MC-4, the exceptionally small chalcopyrite crystals (<10 nm) are shown forming circular to spherical clusters (Fig. 4) and are, of course, a completely different morphology than the large, massive, and weathered chalcopyrites seen in the floodplain. Zn, As, and Pb are also present in these secondary sulfides. The Zn may be from intergrowths of sphalerite (chalcopyrite and sphalerite electron diffraction ring patterns are difficult to distinguish), and the As and Pb are probably substituting in these sulfide structures, although we cannot rule out additional traces of As- and Pb-containing sulfides. The point is, though, that the re-formation of sulfides in the anoxic riverbeds is taking up highly toxic metals like As and Pb. In MC-4, we also saw the formation of nanocrystalline sphalerite with small amounts of As and Pb present (Fig. 7b). In KB-4, the Zn-sulfides shown in Figure 12 also look secondary (that is, forming in the anoxic portions of the riverbed). In this material, Zn and S are the only major elements detected, although there are minor to moderate amounts of Fe, Si, P, Cl, and Ca. The

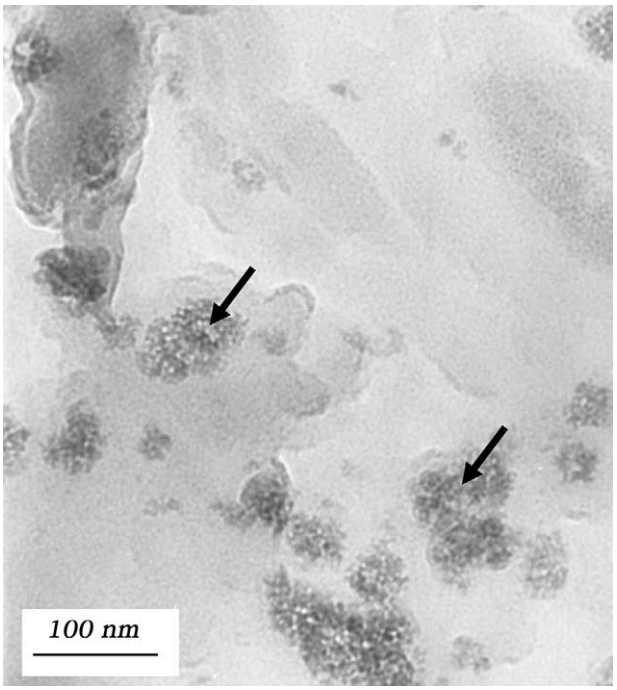

Fig. 12. Exceptionally fine Zn-sulfide particles, seemingly aggregated in clumps (examples denoted by arrows), as well as Zn-sulfide films (covering much of the remaining field of view, and distinguished by different shades of gray). A diffraction pattern could not be obtained anywhere in this image area. This material is from the riverbed at Kohr's Bend (KB-4).

lack of any diffraction pattern within the field of view of Figure 12 indicates that this Zn-sulfide is not yet structurally ordered.

The riverbed formation of these sulfides described above is very likely the result of sulfate-reducing bacteria, as described, for example, in Ledin and Pedersen (1996), Labrenz et al. (2000), and Druschel et al. (2002). The stability of heavy metals in these sulfides is important in their bioavailability. Crystals in the nanosize regime generally have considerably different properties than the same crystals that are larger due to variations in their electronic and surface properties (Madden and Hochella, 2005). Although at this time we can only speculate, nanocrystals of chalcopyrite or sphalerite may be considerably more reactive than larger crystals of the same minerals. This may be important, for example, when such small particles are ingested in a benthic organism, or lodged on the gills of a fish. We predict that toxic metals in these nanophases are far more bioavailable than from larger crystals of the same mineral due to enhanced solubility of the former (Hochella, 2002).

Acknowledgments—Constructive reviews were kindly provided by Kenneth Livi, Dan Strawn, and two anonymous reviewers. These reviews significantly improved the manuscript. The authors are grateful to Ulla Heitmann for outstanding contributions to the TEM sample preparation. MFH is grateful for the generosity and support of the Institüt für Mineralogie and Interdisciplinary Centre for Electron Microscopy and Microanalysis, Universität Münster, as well as valuable assistance from Jose Manuel Astilleros, Udo Becker, Ute Golla, Jürgen Löns, Hinrich-Wilhelm Meyer, Kilian Pollok, and Michael Schindler. Major funding for this work, generated in conjunction with a sabbatical leave for MFH in the Putnis labs, was granted in the form of a Humboldt Research Award from the Alexander von Humboldt Foundation, Bonn, Germany, and also by a sabbatical grant from Virginia Tech. Important additional research funding was provided by NSF grant EAR-01-03053 and DOE grant DE-FG02-02ER15326. The experimental facilities at Münster are supported by grants from the Deutsche Forschungsgemeinschaft (DFG).

Associate editor: D. Sparks

REFERENCES

Alpers C. N., Blowes D. W., Nordstrom D. K., and Jambor J. L. (1994) Secondary minerals and acid-mine water chemistry. In *Short Course Handbook on Environmental Geochemistry of Sulfide Mine Wastes* (ed. J. L. Jambor and D. W. Blowes), pp. 247–270, Mineralogical Association of Canada.

Axtmann E. V. and Luoma S. N. (1991) Large scale distribution of metal contamination in the fine-grained sediments of the Clark Fork River, Montana, USA. *Appl. Geochem.* **6,** 75–88.

Benjamin M. M. and Leckie J. O. (1981a) Multiple-site adsorption of Cd, Cu, Zn and Pb on amorphous iron oxyhydroxide. *J. Colloid Interface Sci.* **79,** 209–221.

Benjamin M. M. and Leckie J. O. (1981b) Competitive adsorption of Cd, Cu, Zn and Pb on amorphous iron oxyhydroxides. *J. Colloid Interface Sci.* **83,** 410–419.

Bigham J. M. (1994) Mineralogy of ochre deposits formed by sulfide oxidation. In *Short Course Handbook on Environmental Geochemistry of Sulfide Mine-Wastes* (ed. J. L. Jambor and D. W. Blowes), pp. 103–132, Mineralogical Association of Canada.

Bigham J. M. and Nordstrom D. K. (2000) Iron and aluminum hydroxysulfates from acid sulfate water. In *Sulfate Minerals: Crystallography, Geochemistry, and Environmental Significance,* Reviews in Mineralogy, Vol. 40 (ed. C. N. Alpers et al.), pp. 351–403, Mineralogical Society of America.

Chung F. H. (1974) Quantitative interpretation of X-ray diffraction patterns of mixtures. I. Matrix flushing method for quantitative multicomponent analysis *J. Appl. Crystal.* **7,** 519–525.

DaRosa C. D. and Lyon J. S. (1997) Hardrock mining and water: An overview. In *Golden Dreams, Poisoned Streams* (ed. P.M. Hocker), pp. 3–24, Mineral Policy Center.

Druschel G. K., Labrenz M., Thomsen-Ebert T., Fowle D. A., and Banfield J. F. (2002) Geochemical modeling of ZnS in biofilms: An example of ore depositional processes. *Econ. Geol.* **97,** 1319–1329.

Eberl D. D. (2003) User guide to RockJock - A program for determining quantitative mineralogy from X-ray diffraction data. U.S. Geological Survey Open File Report 03-78.

Hochella M. F., Jr. (2002) Nanoscience and technology: The next revolution in the Earth sciences. *Earth Planet. Sci. Let.* **203,** 593–605.

Hochella M. F., Jr., Moore J. N., Golla U., Putnis A. (1999) A TEM study of samples from acid mine drainage systems: Metal-mineral association with implications for transport. *Geochem. Cosmochim. Acta* **63,** 3395–3406.

Hochella M. F., Jr., Kasama T., Putnis A., Putnis C., and Moore J. N. Environmentally important, poorly crystalline Fe/Mn hydrous oxides: Ferrihydrite and a possibly new vernadite-like mineral from the Clark Fork River Superfund Complex. *Amer. Mineral.* (in press)

Hudson-Edwards K. A., Macklin M. G., Jamieson H. E., Brewer P. A., Coulthard T. J., Howard A. J., and Turner J. N. (2003) The impact of tailings dam spills and clean-up operations on sediment and water quality in river systems: the Ríos Agrio-Guadiamar, Aznalcóllar, Spain. *Appl. Geochem.* **18,** 221–239.

Jambor J. L. and Blowes D. W., eds. (1994) Short Course Handbook on Environmental Geochemistry of Sulfide Mine-Wastes. Mineralogical Association of Canada.

Kimball B. A., Broshears R. E., Bencala K. E., and McKnight D. M. (1994) Coupling of hydrologic transport and chemical reactions in a stream affected by acid mine drainage. *Environ. Sci. Technol.* **28,** 2065–2073.

Labrenz M., Druschel G. K., Thomsen-Ebert T., Gilbert B., Welch S. A., Kemner K. M., Logan G. A., Summons R. E., De Stasio G., Bond P. L., Lai B., Kelly S. D., and Banfield J. F. (2000) Formation

of sphalerite (ZnS) deposits in natural biofilms of sulfate-reducing bacteria. *Science* **290,** 1744–1747.

Ledin M. and Pedersen K. (1996) The environmental impact of mine wastes–Roles of microorganisms and their significance in treatment of mine wastes. *Earth-Science Rev.* **41,** 67–108.

Lejeune K., Galbraith H., Lipton J., and Kaputska L. (1996) Effects of metal and arsenic on riparian communities in southwest Montana. *Ecotoxicology* **5,** 297–312.

Luoma S. N. and Carter J. L. (1991) Effects of trace metals on aquatic benthos. In *Metal Ecotoxicology, Concepts and Applications* (ed. C. Newman and A.W. McIntosh), pp. 261–300, Lewis Publishers.

Madden A. and Hochella M. F., Jr. (2005) A test of geochemical reactivity as a function of mineral size: Manganese oxidation promoted by hematite nanoparticles. *Geochim. Cosmochim. Acta* **69,** 389–398.

Manceau A., Lanson B., and Drits V. A. (2002) Structure of heavy metal sorbed birnessite. Part III: Results from powder and polarized extended X-ray absorption fine structure spectroscopy. *Geochim. Cosmochim. Acta* **66,** 2639–2663.

Maron D. C. (1989) Physical and chemical characteristics of a metal-contaminated overbank deposit, west-central South Dakota, USA. *Earth Surface Processes Landforms* **14,** 419–432.

Meyer C., Shea E. P., and Goddard C. C. (1968) Ore deposits at Butte, Montana. In *Ore Deposits of the United States, 1933–1967,* Vol. 2 (ed. J. O. Ridge), pp. 1363–1416, American Institute of Mining, Metallurgical and Petroleum Engineers.

Miller J. R. (1997) The role of fluvial geomorphic processes in the dispersal of heavy metals from mine sites. *J. Geochem. Exploration* **58,** 101–118.

Moore J. N. and Luoma S. N. (1990) Hazardous wastes from large-scale metal extraction: A case study. *Environ. Sci. Technol.* **24,** 1278–1285.

O'Reilly S. E. and Hochella M. F., Jr. (2003) Lead sorption efficiencies of natural and synthetic Mn and Fe-oxides. *Geochem. Cosmochim. Acta* **67,** 4471–4487.

Page R. and Wenk H. R. (1979) Phyllosilicate alteration of plagioclase studied by transmission electron microscopy. *Geology* **7,** 393–397.

Post J. E. (1999) Manganese oxide minerals: Crystal structures and economic and environmental significance. *Proceed. Nat. Acad. Sci. USA* **96,** 3447–3454.

Smith D. K., Johnson G. G., Jr., Scheible W., Wims A. M., Johnson J. L., and Ullmann G. (1987) Quantitative X-ray powder diffraction method using the full diffraction pattern. *Powder Diffraction* **2,** 73–77.

Srodon J., Drits V. A., McCarty D. K., Hsieh J. C. C., and Eberl D. D. (2001) Quantitative X-ray diffraction analysis of clay-bearing rocks from random preparations. *Clays Clay Minerals* **49,** 514–528.

Stoffregen R. E., Alpers C. N., and Jambor J. L. (2000) Alunite-jarosite crystallography, thermodynamics, and geochronology. In *Sulfate Minerals: Crystallography, Geochemistry, and Environmental Significance,* Reviews in Mineralogy, Vol. 40 (ed. C. N. Alpers et al.), pp. 453–479, Mineralogical Society of America.

Swanson B. J. (2002) *Bank Erosion and Metal Loading in a Contaminated Floodplain System, Upper Clark Fork River Valley, Montana.* M.S. Thesis, University of Montana.

U.S. Environmental Protection Agency (1985) *Wastes From the Extraction and Beneficiation of Metallic Ores, Phosphate Rock, Asbestos, Overburden From Uranium Mining and Oil Shale.* EPA Report to Congress, December 31, 1985, 4–49.

Williams D. B. and Carter C. B. (1996) *Transmission Electron Microscopy, A Textbook for Materials Science.* Plenum Press.